Machine Learning-Based Angle of Arrival Estimation for Ultra-Wide Band Radios

Mostafa Naseri, Adnan Shahid, Gert-Jan Gordebeke, Sam Lemey, Michiel Boes, Samuel Van de Velde, and Eli De Poorter

***Abstract*—This paper analyzes the feasibility of deep convolutional neural networks (DCNN) for accurate ultra-wideband (UWB) angle of arrival estimation that is robust against hardware imperfections. To this end, a uniform linear array with four antenna elements is leveraged and a DCNN approach is proposed and compared with traditional approaches, such as MUSIC and phase difference of arrival estimators, for different environments, number of available channel impulse responses, and polarization mismatches, in terms of absolute value of error and computational complexity. The proposed approach outperforms the traditional approaches up to 80° error reduction at a computational complexity increase of only 10% compared to MUSIC.**

***Index Terms*—Angle of arrival (AoA), ultra-wideband (UWB), channel impulse response (CIR), machine learning (ML), deep convolutional neural network (DCNN), PDoA, MUSIC.**

I. Introduction

ULTRA-wideband (UWB) has become a key technology for localization systems in GPS-denied environments [1], [2]. The UWB technology benefits from a high time-domain resolution leading to a precise time of flight (ToF) and high-resolution channel impulse response (CIR) measurements. The high resolution CIR provides useful information that could be used to tackle main localization challenges, e.g. multipath propagation, making UWB a key technology for challenging environments.

The UWB technology enables several localization approaches, among which angle of arrival (AoA) estimation is highly demanded. AoA estimation is a crucial task in narrow beam wireless data transmission and smart antenna systems to facilitate beamforming [3], vehicle to vehicle communication [4], and indoor positioning [5]. Unlike approaches that require two-way communication between anchor node and tag node, e.g. two-way ranging, in AoA estimation a feedback link is not required (in self localization) which results in better system scalability and complexity. In addition, current UWB positioning systems typically use timing information to determine the distance between a mobile tag and several distributed anchor nodes. By adding an additional antenna and radio module on the anchor node (e.g. creating an antenna array), the phase and arrival time can be determined at each antenna element, enabling the extraction of angle-of-arrival information. Hence, using AoA, the total required infrastructure cost can be reduced significantly.

Traditional AoA estimation methods are divided into several categories, namely spectral-based estimation, deterministic parameter estimation, and subspace-based AoA estimation [6]. These methods are vulnerable to array imperfections caused by suboptimal antenna design, fabrication imperfections, inter-antenna interference, and installation platform effects. In addition, challenging environmental effects, e.g. multipath and non-line of sight (NLoS), will degrade the performance of these traditional methods [7]. Modeling all of the aforementioned destructive effects is not necessarily an efficient approach, if not impractical.

As opposed to the rule-based algorithms, a deep convolutional neural network (DCNN) is adopted in this work. DCNNs select features from the input without manual feature extraction and finds a mapping from the features in the observed data to the desired output, i.e. true AoA. DCNNs have demonstrated excellent performance in the image processing domain [8]. The DCNN can overcome modeling complications of the aforementioned antenna array imperfections and extract features from the antenna array output to make the algorithm robust against environmental changes. It should be noted that relying on simulation results for evaluating machine learning (ML) solutions could be misleading due to the fact that in the simulations, the interfering effects are artificially added to the system using known models [9]. However, such imperfections could be unknown, difficult to measure, or too complicated to be modeled. In this work, we use supervised ML to estimate the AoA from a set of labeled input-output pairs.

Although almost all AoA estimation methods rely on the reception of the signal by an array of antennas (or one antenna that moves to different positions), [10] and [11] propose a single-antenna AoA estimation approach. Single antenna AoA estimation algorithms either require more complicated hardware [10] or exploit the angle-dependent property of the transmitter and receiver antenna pattern [11]. In the latter approach, the AoA estimator maps the CIR to AoA for one specific convolution of the impulse response of the transmit antenna, channel, and receive antenna. Since in this approach the estimator does not have access to differential information (between antenna elements), the mapping is environment-dependent for a fixed pair of transmit and receive antennas.

In addition to the error performance of the adopted algorithm, its complexity plays an important role in an AoA estimation, especially for real-time applications [12]. For instance, iterative searches or singular value decomposition (SVD) increase the complexity of an algorithm and, hence, require a

Mostafa Naseri, Adnan Shahid, Gert-Jan Gordebeke, Sam Lemey, and Eli De Poorter are with IDLab, Department of Information Technology, Ghent University - imec, Ghent, Belgium (email: mostafa.naseri@ugent.be; adnan.shahid@ugent.be; gertjan.gordebeke@ugent.be; sam.lemey@ugent.be; eli.depoorter@ugent.be).

Michiel Boes and Samuel Van de Velde are with Pozyx, Ghent, Belgium (email: michiel.boes@pozyx.io; samuel@pozyx.io).

careful examination of the time complexity. Furthermore, lack of adequate snapshots can severely affect the AoA estimation algorithm [13] hence, evaluation of the algorithm performance in absence of adequate CIRs is of major importance to acquire insight on a system level.

In this paper, a supervised ML approach is proposed to achieve accurate AoA estimation robust against hardware imperfections. It is validated for clean, multipath, and high-noise conditions in various environments through experimental results obtained by a four-antenna uniform linear array (ULA). While prior work supported by empirical data is limited to single and double antenna setups, our estimator is extendable to any array configuration. The antenna array hardware is equipped with four synchronized Decawave DW1000 chips to extract the CIR at each antenna element. The main contributions of this paper are as follows:

- A supervised DCNN solution is proposed to improve AoA estimation error in multi-antenna-based UWB systems. The model is trained via high granularity labeled data captured in an anechoic chamber. The model takes the amplitude of the truncated CIR as input and outputs the estimated AoA.
- Comparison of different AoA estimation algorithms in terms of estimation error distribution and complexity. In particular, the proposed method is compared to the phase difference of arrival (PDoA) and MUSIC algorithms.
- Analysis of the robustness of the proposed solution against small numbers of observed CIRs and antenna polarization mismatch and comparison with PDoA- and MUSIC-based AoA estimation.

II. System Description

Consider a single-antenna transmitter and multi-antenna receiver setup in an environment with N_{path} paths arriving at the i-th receiver antenna element. The real-valued channel impulse response is given by,

$$h_i(\tau) = \sum_{n=1}^{N_{path}} \alpha_n r_n(\tau) \otimes \delta(\tau - \tau_n) \tag{1}$$

where α_n and τ_n are the gain and delay of the n-th path, $r_n(\tau)$ is the pulse distorted due to interaction on the way from transmitter to receiver, $\otimes$ is the convolution operator, and $\delta(\cdot)$ is a Dirac function [14]. The shape of the distorted pulse $r_n(\tau)$, depends on the transmitted pulse, the transmit antenna's impulse response h_{TX}, the channel (excluding antennas) impulse response h_H, and the receive antenna's impulse response h_{RX}. h_{TX}, h_H, and h_{RX} are cascaded blocks that could be combined together depending on assumptions on the environment and antennas [15, Sec. 4.2]. For the specific case of linear time invariant (LTI) systems, the equivalent system reduces to $h_{TX} \otimes h_H \otimes h_{RX}$ which is valid for static environments. Note that dependence of $h_i(\cdot)$, α, τ, and r on the angle of departure from the transmit antenna and angle of arrival of the receive antenna is omitted for simplicity of the notations.

A. Dataset Generation and Description

The hardware setup, shown in Fig. 1, consists of one UWB Pozyx developer tag with an on-board chip antenna [16], and one anchor board containing four DW1000 chips interconnected to an ultra-wideband 1×4 air-filled substrate-integrated-waveguide (AFSIW) cavity-backed slot antenna array [17]. The DW1000 chips are synchronized by a common clock and the antenna array is interfaced to the PCB.

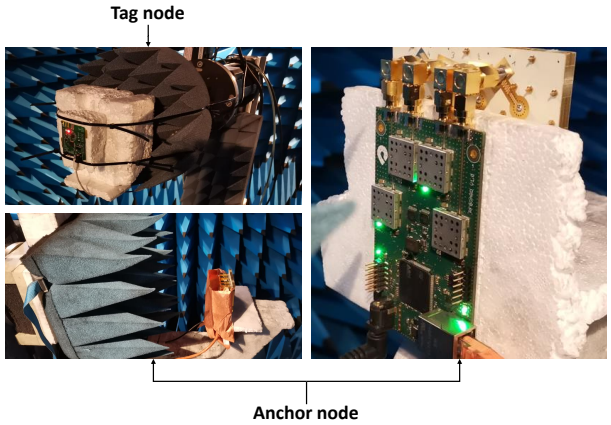

Fig. 1. Single-antenna tag and anchor node with four synchronized DW1000 chips and a 1×4 antenna array in an anechoic chamber.

The experiments are conducted in clean, noisy, and multipath environments. The distance between the anchor and tag node is 2.14 m in all the experiments. In the clean environment experiment, no additional interfering effect is added to the anechoic chamber. In the noisy environment experiment, an extra -10 dB attenuator is added between each antenna/DW1000 pair. Moreover, in the multipath experiment, a reflector surface is used to introduce a second path (LoS and NLoS) to the existing medium. The anechoic chamber is equipped with an NSI-700S spherical near-field scanner suitable for high granularity AoA measurements [18]. 500 CIRs are captured per AoA for [-90°, 90°] with a granularity of 1°. It is worth mentioning that since we use a hemispherical antenna with a high front-to-back ratio to spatially filter away waves impinging from the antenna backside, we choose [-90°, 90°] as the range of interest.

The multi-antenna anchor node communicates the complex-valued samples of the accumulated CIR, FP index of CIR, and synchronization frame delimiter (SFD) at the four DW1000 chips over an Ethernet interface. A CIR is constructed by accumulating the cross-correlation of the arriving preamble sequence and a known sequence with a resolution of 1 ns at each DW1000 chip. The accumulated CIRs have a length of L_{CIR} = 1016 and one can extract the phase of arrival by calculating the phase of the complex-valued CIR at the first path (FP) index. Due to the limited resolution of the CIR, i.e. 1 ns, the FP index may not report the exact arrival moment and as a result, it is recommended that the phase of arrival is calculated by averaging the phase over the FP index and its adjacent samples [10]. Note that the CIR reception rate is not

constant and depends on the quality of the received signal. In our experiment setup, 53 ms is required to capture one CIR.

B. AoA Estimation of UWB Array

In this section, we formulate the AoA estimation problem taking into account the limited training and calibration data, and estimation update rate. The mean absolute error (MAE) of estimates can be defined as follows:

$$MAE(\theta) = \frac{1}{N}\sum_{i=1}^{N}|\theta - \hat{\theta}_i| \tag{2}$$

and

$$\hat{\theta}_i = f(\boldsymbol{g_1^i}, ..., \boldsymbol{g_{N_A}^i}) \tag{3}$$

where N is the number of available estimates per AoA, N_A is the number of antennas in the array, $\theta \in \Theta$ = {-90, -89,..., 90}, $f(\cdot)$ represents the estimation algorithm, and $\boldsymbol{g_{n_A}^i}$ contains N_{CIR} complex-valued CIRs, and the corresponding SFDs and FP indices at antenna n_A. The estimator uses N_{CIR} CIRs, SFDs, and FP indices to generate one update (new estimate). The estimator can use N_{train} of the angles in Θ for training or calibration purposes.

C. Rule-Based Methods

In this work, the proposed DCNN-based method is compared with two rule-based AoA estimation methods, MUSIC, and PDoA. MUSIC is a spectral-based AoA estimation method that uses the covariance matrix of the received signal $\hat{R} = \frac{1}{N_{CIR}}\sum_{N_{CIR}}^{1} y[n]y[n]^H = U_n\Lambda_n U_n + U_s\Lambda_s U_s$, where y is the array output, U_s and U_n are the signal and noise subspaces, Λ_s and Λ_s are diagonal matrices, and $(\cdot)^H$ is the Hermitian transpose. The MUSIC AoA estimate is equivalent to finding the direction that maximizes the MUSIC spectrum given by

$$P(\alpha) = \frac{a(\alpha)^H a(\alpha)}{a(\alpha)^H U_n U_n^H a(\alpha)} \tag{4}$$

where α is the direction of arrival and $a(\cdot)$ is the steering vector [6]. PDoA AoA estimation works based on the difference between the phase at adjacent antennas with a separation below half wavelength. The AoA estimate is given by

$$\hat{\theta} = \frac{1}{\beta}\arcsin\frac{\gamma}{\pi} \tag{5}$$

where γ is a function of PDoA and SFD of the two receivers, and β depends on the antenna array (in this work $\beta = \frac{1}{0.87}$) [19]. Note that since PDoA is only applicable to two antennas, we average three AoA estimates obtained from each subarray of two adjacent antennas in the 1×4 antenna array.

D. ML-Based AoA Estimation

Table I gives an overview of the proposed algorithm. The network estimates the AoA using the magnitude of windowed CIRs received by each antenna element. The magnitude of each CIR is windowed over the [FP-5, FP+30] index range. The optimal range depends on the interests in the multipath components of the CIR in the specific application. Our evaluations show that although the CIR phase conveys important information about the AoA, our proposed method achieves the same performance in terms of MAE using only the CIR's magnitude; thereby reducing the number of parameters in the network.

TABLE I. PROPOSED ESTIMATOR ARCHITECTURE

Layer	Type	Description	Layer	Type	Description
0	Input	35×4	10	dropout	0.5
1	Conv1D	64×(size=3) + RELU	11	flatten	-
2	Conv1D	64×(size=3) + RELU	12	Dense	256 + RELU
3	max pooling	size=4	13	Dense	256 + RELU
4	norm	-	14	Dense	256 + RELU
5	dropout	0.5	15	Dense	256 + RELU
6	Conv1D	32×(size=3) + RELU	16	Dense	256 + RELU
7	Conv1D	256×(size=3) + RELU	17	dropout	0.5
8	max pooling	size=4	18	Linear	Output
9	norm	-			

The proposed CNN uses two 1D convolutional layers to detect features in the input vectors, each followed by a rectified linear unit (RELU), a max pooling, and a dropout layer. A similar combination of layers is adopted in layers 6 and 7 as reported in Table I, and the output is flattened to form the input to the dense layers. In addition to the dropout layers used after the convolutional layers, a dropout layer is used after dense layer 16. These layers prevent a small number of the extracted features to dominate the generation of the output (AoA estimate) by randomly setting some features to zero at each training step. We avoid providing mathematical formulas for each layer due to the limited length of this letter.

A total number of 90500 CIRs are used for training, validation, and test of the network. Instead of randomly selecting from a pool of CIR samples for test, train, and validation, we divide Θ into three subsets, i.e. Θ_{test}, Θ_{train}, and $\Theta_{validation}$. This ensures the proposed DCNN has not observed any CIR from the directions selected for testing the proposed method. Furthermore, test, train, and validation consist of 15%, 70%, and 15% of the angles in Θ, respectively. The proposed DCNN has 439,329 trainable parameters, and Adam optimizer is adopted for training of the network [20].

III. EXPERIMENTAL RESULTS

In this section, we evaluate the performance of the proposed estimator in terms of MAE and the absolute value of error. All estimators are calibrated or trained for each test environment separately to evaluate the generalization of each algorithm to unseen AoAs. Fig. 2 depicts the average performance of PDoA, MUSIC, and our ML-based solution in different test environments for N_{CIR}=5. As depicted in Fig. 2a, the average performance of our proposed method outperforms PDoA and MUSIC over the range [-90°, 90°]. Note that except reference angle of arrivals mentioned in Table II, other test AoAs are selected randomly. In addition to the non-linearity that both PDoA and MUSIC algorithms suffer from around extreme angles, MUSIC shows outliers and clipping to 90° and -90°. It is worth mentioning that although [19] proposes using a lookup table to overcome the nonlinearity around extreme angles for PDoA, Figs. 2b and 2c show that a one-to-one relationship between the estimated AoA and true AoA does not exist for a wide range of AoAs. To further investigate the distribution of the absolute value of the estimation error, the 50th, 90th, and 99th percentiles of the absolute value of error

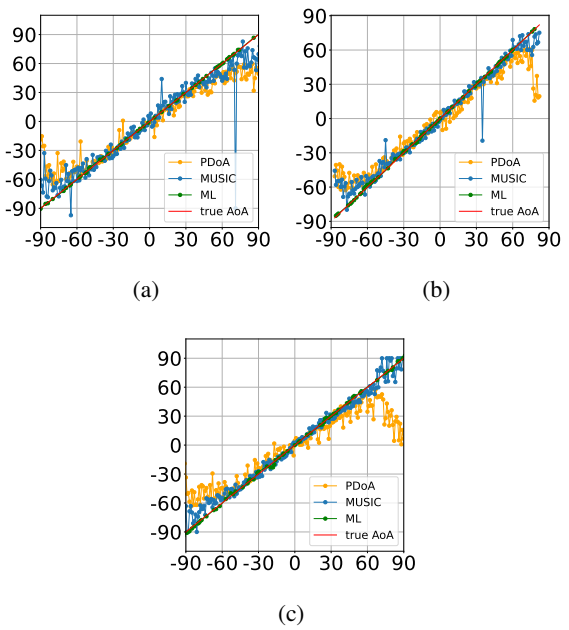

Fig. 2. Rule-based and ML-based AoA estimation in clean (a), noisy (b), and multipath (c) environments for $N_{CIR} = 5$.

are reported in Table II for N_{CIR}=5. The AoA estimation error is a function of true AoA due to the planar array configuration. Therefore, the error percentiles are reported for {-90, -60, -30, 0, 30, 60, 90}, showcasing that our proposed solution has a 99th percentile below or equal to 2.2°, 2.8°, and 2.2° for the clean, noisy, and multipath environments. These error percentile values for different AoAs show that, in addition to the general improvement, the performance of our proposed method is not degraded for extreme AoAs, in contrast to the more conventional rule-based methods.

The number of CIRs used to produce one AoA estimate, N_{CIR}, has an impact on the design of AoA estimation and tracking systems. For instance, using N_{CIR} = 5 takes 267 ms on average in the clean environment experiment to generate one AoA estimate update. As a result, N_{CIR} determines the maximum angular maneuver velocity that the algorithm can capture, as well as the power consumption. Fig. 3 illustrates how N_{CIR} affects the 95th percentiles of the absolute value of error in PDoA, MUSIC, and our proposed method. For smaller values of N_{CIR}, it is more likely that MUSIC gives highly erroneous estimates, especially for extreme AoAs. PDoA on the other hand is less sensitive to N_{CIR} in terms of producing extremely erroneous estimates.

A polarization mismatch between the antenna elements in the array and the incident electromagnetic wave can distort both the amplitude and the phase of the received signal. In order to analyse the effectiveness of the proposed ML-based method against polarization mismatch, we conducted measurements for 0°, 45°, 75°, 85° polarization mismatch in the clean environment condition. Fig. 4 shows the average performance of the AoA estimation techniques for the aforementioned polarization mismatches. Both the MUSIC and PDoA fail to compensate for the polarization mismatch despite the fact that

TABLE II. ABSOLUTE VALUE OF ERROR PERCENTILES FOR N_{CIR} = 5

(a) CLEAN ENVIRONMENT

AoA	MUSIC			PDoA			ML		
	50th	90th	99th	50th	90th	99th	50th	90th	99th
-90°	20.8°	32.0°	180.0°	70.2°	78.8°	80.7°	0.8°	1.3°	1.7°
-60°	5.8°	14.3°	24.6°	10.2°	18.2°	26.7°	0.4°	1.4°	2.2°
-30°	3.6°	7.7°	12.5°	1.2°	9.5°	16.9°	0.5°	1.4°	1.9°
0°	2.6°	6.9°	11.4°	1.4°	7.9°	10.36°	0.5°	0.9°	1.4°
30°	4.1°	8.6°	48.3°	1.9°	8.5°	17.6°	0.5°	1.0°	2.0°
60°	9.4°	17.6°	22.5°	9.4°	18.6°	31.9°	0.5°	1.1°	1.5°
90°	24.9°	34.8°	180.0°	58.6°	72.7°	79.6°	0.7°	1.2°	1.5°

(b) NOISY ENVIRONMENT

AoA	MUSIC			PDoA			ML		
	50th	90th	99th	50th	90th	99th	50th	90th	99th
-90°	31.2°	36.4°	180.0°	36.9°	51.8°	65.3°	2.2°	2.5°	2.8°
-60°	4.0°	10.1°	13.6°	6.6°	16.1°	25.2°	0.4°	1.4°	1.9°
-30°	2.1°	4.4°	5.2°	0.9°	8.6°	12.7°	0.5°	1.4°	2.4°
0°	2.0°	4.4°	6.4°	0.7°	5.6°	10.8°	0.4°	0.9°	1.5°
30°	1.7°	4.5°	7.1°	2.5°	7.8°	16.9°	0.4°	0.9°	1.0°
60°	4.2°	8.9°	20.6°	4.2°	13.0°	18.1°	0.3°	0.8°	1.0°
90°	10.1°	21.7°	180.0°	63.5°	78.6°	87.2°	0.8°	1.1°	1.4°

(c) MULTIPATH ENVIRONMENT

AoA	MUSIC			PDoA			ML		
	50th	90th	99th	50th	90th	99th	50th	90th	99th
-90°	10.1°	24.5°	180.0°	65.3°	76.6°	81.8°	0.3°	0.8°	0.9°
-60°	5.4°	10.8°	13.7°	11.3°	21.2°	25.6°	0.4°	0.7°	1.2°
-30°	2.2°	6.1°	10.4°	3.0°	11.4°	16.2°	0.6°	1.7°	2.2°
0°	2.4°	4.7°	6.4°	0.9°	5.9°	10.7°	0.2°	0.4°	0.5°
30°	2.6°	6.2°	7.4°	4.5°	13.4°	22.6°	0.2°	0.3°	0.4°
60°	7.2°	11.8°	14.4°	16.5°	31.2°	36.2°	0.2°	0.4°	0.6°
90°	11.9°	22.2°	147.1°	52.5°	73.1°	84.5°	0.2°	0.4°	0.6°

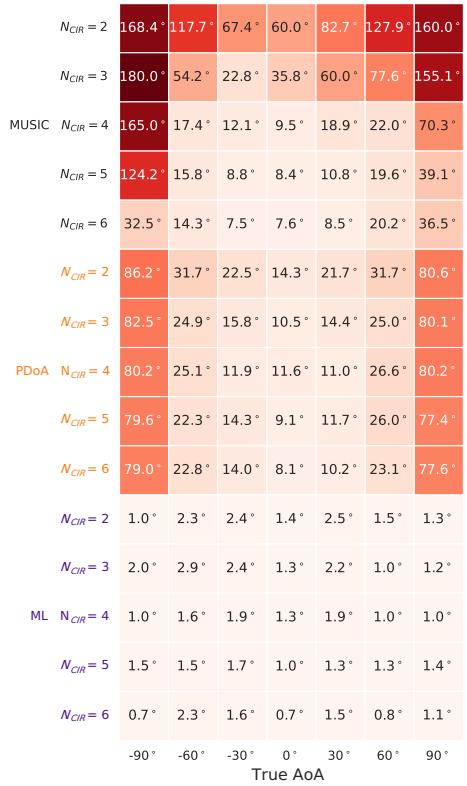

Fig. 3. The 95th percentile of the absolute value of the AoA estimation error is shown for different values of N_{CIR} in a clean environment. For each AoA, 500 CIRs are used to form the empirical CDF.

they were re-calibrated for each polarization independently. The proposed ML-based estimator, PDoA, and MUSIC are

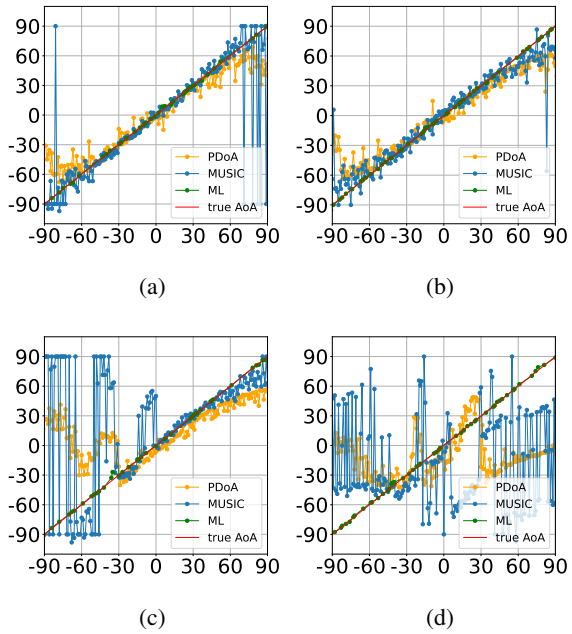

Fig. 4. Effect of polarization mismatch on AoA estimation algorithms. The average AoA estimation performance is depicted for N_{CIR} = 5 and polarization mismatch 0° (a), 45° (b), 75° (c), and 85° (d).

compared in Table III in terms of average execution time in milliseconds for different values of N_{CIR}. The proposed method has almost the same execution time as MUSIC. PDoA, however, has a shorter execution time (approximately 0.07 ms) as expected for its simple structure shown in eq. 5. We average the execution time over 1000 runs on a device equipped with a 6 core Intel Core i7 CPU at 2.7 GHz, and 16 GB RAM using the *timeit* Python module [21].

TABLE III. AVERAGE EXECUTION TIME (MS)

N_{CIR}	PDoA	MUSIC	ML
2	0.069	19.999	22.946
3	0.071	21.243	23.174
4	0.072	21.551	23.267
5	0.073	21.685	23.464
6	0.074	22.005	23.903

IV. CONCLUSION

This paper proposed a DCNN-based AoA estimator for multi-antenna UWB systems. The proposed solution has a 99th percentile error of 2.8°, compared to 180° and 84.5° for MUSIC and PDoA, respectively. Furthermore, while decreasing N_{CIR} from 6 to 2 worsens the 95th percentile of the error for the traditional approaches such as MUSIC (from 36.5° to 168.4°) and PDoA (from 79.0° to 86.2°). The proposed solution is more robust and the errors do not exceed 2.5°. Moreover, the proposed solution is shown to effectively solve the polarization mismatch. Finally, although the results show significant error improvements, the proposed approach has almost the same execution time as the traditional approaches.

REFERENCES

[1] A. Khan, S. Wang, and Z. Zhu, "Angle-of-arrival estimation using an adaptive machine learning framework," *IEEE Communications Letters*, vol. 23, no. 2, pp. 294–297, 2019.

[2] F. M. Martel, J. Sidorenko, C. Bodensteiner, and M. Arens, "Augmented reality and UWB technology fusion: Localization of objects with head mounted displays," *Proceedings of the 31st International Technical Meeting of The Satellite Division of the Institute of Navigation (ION GNSS 2018)*, 2018.

[3] M. Wang, F. Gao, S. Jin, and H. Lin, "An overview of enhanced massive MIMO with array signal processing techniques," *IEEE Journal of Selected Topics in Signal Processing*, vol. 13, no. 5, pp. 886–901, 2019.

[4] M. Yang, B. Ai, R. He, C. Huang, Z. Ma, Z. Zhong, J. Wang, L. Pei, Y. Li, and J. Li, "Machine-learning-based fast angle-of-arrival recognition for vehicular communications," *IEEE Transactions on Vehicular Technology*, vol. 70, no. 2, pp. 1592–1605, 2021.

[5] A. Alarifi, A. Al-Salman, M. Alsaleh, A. Alnafessah, S. Al-Hadhrami, M. A. Al-Ammar, and H. S. Al-Khalifa, "Ultra wideband indoor positioning technologies: Analysis and recent advances," *Sensors*, vol. 16, no. 5, 2016. [Online]. Available: https://www.mdpi.com/1424-8220/16/5/707

[6] H. Krim and M. Viberg, "Two decades of array signal processing research: the parametric approach," *IEEE Signal Processing Magazine*, vol. 13, no. 4, pp. 67–94, 1996.

[7] S. Wielandt and L. D. Strycker, "Indoor multipath assisted angle of arrival localization," *Sensors*, vol. 17, no. 11, 2017. [Online]. Available: https://www.mdpi.com/1424-8220/17/11/2522

[8] L. C. Chen, G. Papandreou, I. Kokkinos, K. Murphy, and A. L. Yuille, "Deeplab: Semantic image segmentation with deep convolutional nets, atrous convolution, and fully connected crfs," *IEEE Transactions on Pattern Analysis and Machine Intelligence*, vol. 40, no. 4, pp. 834–848, 2018.

[9] Z. M. Liu, C. Zhang, and P. S. Yu, "Direction-of-arrival estimation based on deep neural networks with robustness to array imperfections," *IEEE Transactions on Antennas and Propagation*, vol. 66, no. 12, pp. 7315–7327, 2018.

[10] N. Smaoui, M. Heydariaan, and O. Gnawail, "Single-antenna AoA estimation with UWB radios," in *2021 IEEE Wireless Communications and Networking Conference (WCNC)*, 2021, pp. 1–7.

[11] A. Ledergerber and R. D'Andrea, "Ultra-wideband angle of arrival estimation based on angle-dependent antenna transfer function," *Sensors*, vol. 19, no. 20, 2019. [Online]. Available: https://www.mdpi.com/1424-8220/19/20/4466

[12] H. Huang, J. Yang, H. Huang, Y. Song, and G. Gui, "Deep learning for super-resolution channel estimation and DOA estimation based massive MIMO system," *IEEE Transactions on Vehicular Technology*, vol. 67, no. 9, pp. 8549–8560, 2018.

[13] Y. Yao, H. Lei, and W. He, "A-CRNN-based method for coherent DOA estimation with unknown source number," *Sensors*, vol. 20, no. 8, 2020. [Online]. Available: https://www.mdpi.com/1424-8220/20/8/2296

[14] A. F. Molisch, "Ultra-wide-band propagation channels," *Proceedings of the IEEE*, vol. 97, no. 2, pp. 353–371, 2009.

[15] M. C. Jeruchim, P. Balaban, and K. S. Shanmugan, *Simulation of Communication Systems: Modeling, Methodology and Techniques*, 2nd ed. USA: Kluwer Academic Publishers, 2000.

[16] Pozyx. [Online]. Available: https://www.pozyx.io/

[17] G. Singh, E. Allebes, Y. He, E. Tiurin, P. Mateman, J. F. Dijkhuis, G.-J. van Schaik, E. Bechthum, J. van Heuvel den, M. El Soussi, A. Breeschoten, H. Korpela, G.-J. Gordebeke, S. Lemey, C. Bachmann, and Y.-H. Liu, "An IR-UWB IEEE 802.15.4z compatible coherent asynchronous polar transmitter in 28-nm CMOS," *IEEE Journal of Solid-State Circuits*, pp. 1–1, 2021.

[18] Electromagnetism. [Online]. Available: https://www.ugent.be/ea/idlab/en/research/research-infrastructure/electromagnetism.htm

[19] I. Dotlic, A. Connell, H. Ma, J. Clancy, and M. McLaughlin, "Angle of arrival estimation using decawave DW1000 integrated circuits," in *2017 14th Workshop on Positioning, Navigation and Communications (WPNC)*, 2017, pp. 1–6.

[20] D. P. Kingma and J. Ba, "Adam: A method for stochastic optimization," *arXiv preprint arXiv:1412.6980*, 2014.

[21] S. Savazzi, M. Nicoli, and V. Rampa, "Federated learning with cooperating devices: A consensus approach for massive IoT networks," *IEEE Internet of Things Journal*, vol. 7, no. 5, pp. 4641–4654, 2020.